JOURNAL OF MATERIALS SCIENCE **37** (2002) 835–844

Normal and anormal microstructure of plasma nitrided Fe-Cr alloys

NOVI GRANITO
Graduate School of Engineering, The University of Tokyo, 7-3-1 Hongo, Tokyo 113-8656, Japan
E-mail: novi@rias.or.jp

HIDEYUKI KUWAHARA
Research Institute for Applied Sciences, Tanaka-Ohicho, Sakyo-ku, Kyoto 606-8202, Japan

TATSUHIKO AIZAWA
Research Center for Advanced Science and Technology, The University of Tokyo, 4-6-1 Komaba, Tokyo 153-8904, Japan

Plasma nitriding behavior of Fe-Cr alloys has been studied at temperatures in the range of 773–873 K in order to provide basic knowledge for microstructure design of nitrided layers and to improve the wear resistance. In the nitriding temperature of 773 K, typical microstructure of nitrided layers was observed as reported elsewhere. However, anormal microstructure of nitrided layers was observed under a nitriding condition, at 873 K for 176.4 ks (49 h). In Fe-13Cr alloy, nitrided layer showed stripe-pattern, each sub-layer of which has different chromium content. Nitrided layer hardness increased gradually from the specimen surface to the nitriding front before dropping drastically to the same level as matrix hardness. The stripe-pattern was also observed for Fe-3Cr alloy at the vicinity of nitriding front for the same nitriding conditions. On the other hand, nitrided layers in Fe-8Cr and Fe-19Cr alloys are composed from different sub-layers, containing different concentration of chromium. These phenomena cannot be explained only by nitrogen diffusion process during the nitriding.

1. Introduction

Among various surface treatments, nitriding technique is always the first candidate to improve hardness, wear resistance and fatigue strength of steels. Recently, the plasma nitriding technique has been widely used in industries, since it has more advantageous items rather than conventional ammonia gas nitriding: e.g. shorter nitriding time, less consumption of gases, easier to control microstructure of nitrided layers [1–4]. However, several problems are still open both in nitriding mechanism and microstructure of nitrided layers [5]. Hence, in order to make comprehensive description of the plasma nitriding mechanism, precise studies on the microstructure of the plasma nitrided layer are necessary.

In usual, nitriding of Fe-alloys or steels results in formation of hard iron nitrided layer with a few micrometers of thickness at the surface. It has been called "external nitriding layer"* or "white layer". The subordinate layer with thickness less than 1 millimeter, is composed of matrix metal with nitrogen atoms and precipitates of iron nitrides and/or nitrides of the alloying elements. It is called "internal nitriding layer"* or "diffusion zone" [6]. Volume fraction and distribution of these nitride precipitates strongly depend on nitriding parameters; for example, nitriding temperature, duration time, gas pressure and properties of matrix alloys [7–9]. Then, it is very important to understand the effect of the above parameters on the nitrided microstructure.

In fact, a new design concept for nitriding is required for further improvement of wear resistance in practice [10]. Remember that a typical nitrided layer should be composed of the external nitriding layer with high hardness and internal nitriding layer with lower hardness. Under severe impact wear condition as reported in Ref. [10], cracks propagate easily from the surface by a heavy impact load, partially because of a residual stress is present at the vicinity of the surface. Hence, a new nitrided surface material structure is needed to reduce the friction coefficient in wear and to improve impact wear resistance, simultaneously. Even aiming for alternative surface nitrided design, plasma nitriding technique must be controlled to search for adaptive nitrided microstructure to the design demand in mechanical properties.

* Both terms of "External nitriding layer" and "Internal nitriding layer" are frequently used in the similar usage as "External oxidation layer" and "Internal oxidation layer", respectively. The same microstructure of nitrided layer as "white layer" in the old time is often called by "compound layer" in recent.

TABLE I Chemical compositions of the specimen used

Alloy	C	Si	Mn	P	S	Cr	Al	Ti	N	O
Fe-3Cr	0.003	0.22	0.01	0.001	0.001	2.98	0.001	0.020	0.0005	0.003
Fe-8Cr	0.002	0.22	0.01	0.001	0.001	7.97	0.001	0.026	0.0006	0.004
Fe-13Cr	0.002	0.22	0.01	0.001	0.001	13.68	0.001	0.026	0.0007	0.004
Fe-19Cr	0.002	0.24	0.01	0.001	0.001	18.64	0.001	0.025	0.0011	0.004

All values are in mass%.

In this study, plasma nitriding temperature was controlled in relatively wide range from 773 K to 873 K in order to investigate several possible microstructures of nitrided layers preferable for heavy impact use. This is based on the prediction that at relatively high nitriding temperature, diffusion of alloying elements might have significant contribution to microstructure control. Four Fe-Cr alloy specimens with different chromium content were prepared homogeneously and plasma nitrided to understand the process and mechanism of plasma nitriding, especially at relatively high temperature region. Optical microscope and X-ray diffraction analysis were utilized to describe microstructure and phases of nitrided layers together with micro-Vickers hardness testing for measurement of hardness distribution on the specimen cross section.

2. Experimental

Ferritic Fe-Cr alloys were used in this work. The chemical compositions are summarized in Table I. The specimens of $10 \times 10 \times 20\,mm^3$ were gradually ground with sandpaper up to the mesh number of 1000 and polished with diamond paste (mean size 1 μm). Then the specimens were rinsed in acetone using an ultrasonic cleaner for 600 s.

The specimens were plasma nitrided under conditions as listed in Table II. Specimens were set on the table as a cathode in nitriding vacuum chamber connected with an anode (ground potential). Specimens were heated up, using heater and hydrogen gas glow discharge simultaneously. The specimen temperature was monitored by a thermocouple, which was inserted into a dummy specimen on the same cathode neighboring to the specimens. At specified nitriding temperature, nitrogen gas was introduced into a chamber at appropriate pressure, and then plasma nitriding started. During nitriding, the gases were evacuated out by a rotary pump to keep gas pressure constant in the chamber.

After nitriding, the specimens were cooled down in hydrogen gas atmosphere until the room temperature and then were cut by micro-cutter into halves to specimen surface. To observe the microstructure of nitrided layer, the cross-section of specimens was mechanically polished and then etched by Nital etchant (90 ml C_2H_5OH + 10 ml HNO_3) for Fe-3Cr and Fe-8Cr and by solution of 5 g $FeCl_2$ + 2ml HCl + 96 ml C_2H_5OH for Fe-13Cr and Fe-19Cr, respectively. Microstructure was observed using an optical microscope. The surface hardness as well as the hardness profiles on the cross-sections of nitrided specimens were measured using micro-Vickers hardness tester. X-ray diffraction was used to identify the phase formed in each nitrided specimen.

TABLE II Plasma nitriding conditions

Temperature (T/K)	773, 823, 873
Time (t/ks)	57.6, 90, 176.4
DC voltage (E/V)	300
Total gas pressure (P/Pa)	532
Gas ratio (R/%)	25%N_2, 75%H_2

3. Experimental results

3.1. Plasma nitriding of Fe-Cr alloys at low temperature

Microstructure of plasma nitrided Fe-Cr alloys at 773 K for 57.6 ks (16 h) is shown in Fig. 1. "S", "F", and "E" in these figures from (a) to (d) denote for the specimen surface, the nitriding front, and the thickness of nitrided layer, respectively. In plasma nitriding, the internal nitriding layer with 50–200 μm in thickness was formed beneath an external nitriding layer with a thickness of 2–3 μm. In the case of plasma nitrided Fe-8Cr, Fe-13Cr and Fe-19Cr, each nitriding front was clearly observed and aligned in parallel with the specimen surface. It indicates that nitriding was driven only by lattice diffusion of nitrogen.

On the other hand, in the case of Fe-3Cr alloy, the boundary between nitrided layer and matrix was not so clear. Thickness of nitrided layers were 230, 140, 105 and 45 μm for Fe-3Cr, Fe-8Cr, Fe-13Cr and Fe-19Cr alloy, respectively. Nitrided layer thickness decreased with increase of chromium content.

Fig. 2a to d summarized hardness profiles in the direction of thickness for four specimens, which were plasma nitrided at 773 K for 57.6 ks (16 h). As commonly seen in Fe-8Cr, Fe-13Cr and Fe-19Cr alloys, surface hardness becomes more than 1000 Hv and remains constant until the nitriding front. Then, hardness reduces at the nitriding front to the same level as the matrix hardness. As shown in Fig. 2(d), the highest surface hardness reached 1200 Hv in Fe-19Cr alloy. Looking through from Fig. 2a to d, the nitriding front, "F", measured in Fig. 1 is corresponding to the point where hardness dropped to the matrix hardness. The transient zone in this hardness distribution is very narrow in Fe-19Cr, but it gradually grows wider with decreasing chromium content.

In Fe-3Cr alloy, the nitrided layer hardness profile in Fig. 2a becomes quite different from those of high chromium content alloys in Fig. 2b to d. Hardness in the nitrided layer becomes nearly constant within 700–800 Hv until the depth of 100 μm from surface. Then it gradually decreases down to the same level as the matrix. To be interested in, this wider transient zone

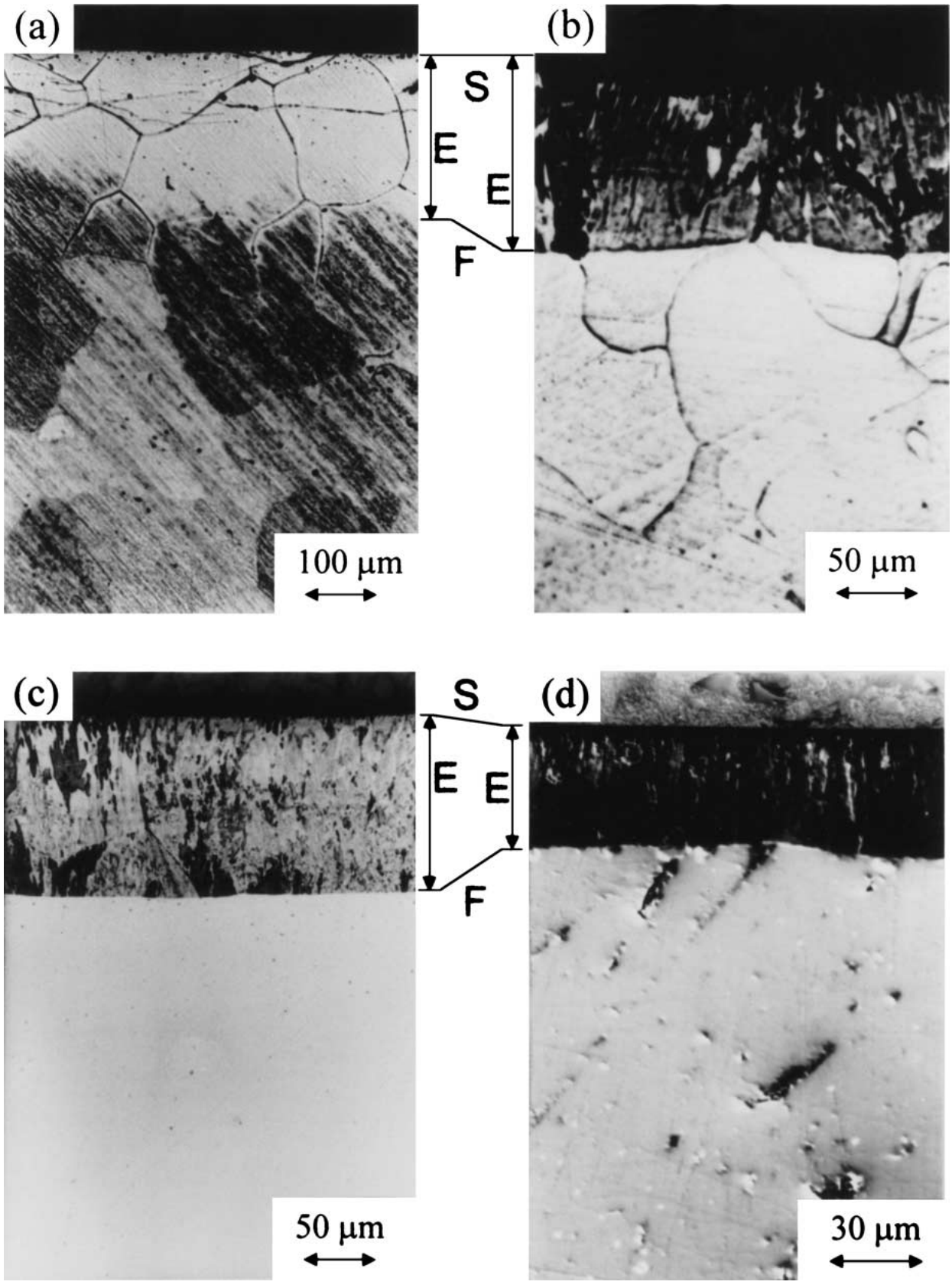

Figure 1 Microstructure of (a) Fe-3Cr, (b) Fe-8Cr, (c) Fe-13Cr and (d) Fe-19Cr alloys as plasma nitrided at 773 K for 57.6 ks.

in the hardness profile in Fe-3Cr alloy is also corresponding to the gray-scale zone at the vicinity of nitriding front in Fig. 1a. This suggests that microstructure as shown in Fig. 1a has proper comparison to the hardness profile in thickness from the surface.

The average hardness in the nitrided layer increases with the chromium content as shown in Fig. 2e. This implies that volume fraction of CrN should increase in the nitrided layer, resulting in enhancement of hardness.

Fig. 3 shows X-ray diffraction pattern on the specimen surface of Fe-Cr alloys plasma nitrided at 823 K for 90 ks (25 h). α-Fe, γ'-Fe_4N and CrN were detected over the whole specimen surface. Strong peak of γ'-Fe_4N indicates that the external nitriding layer is

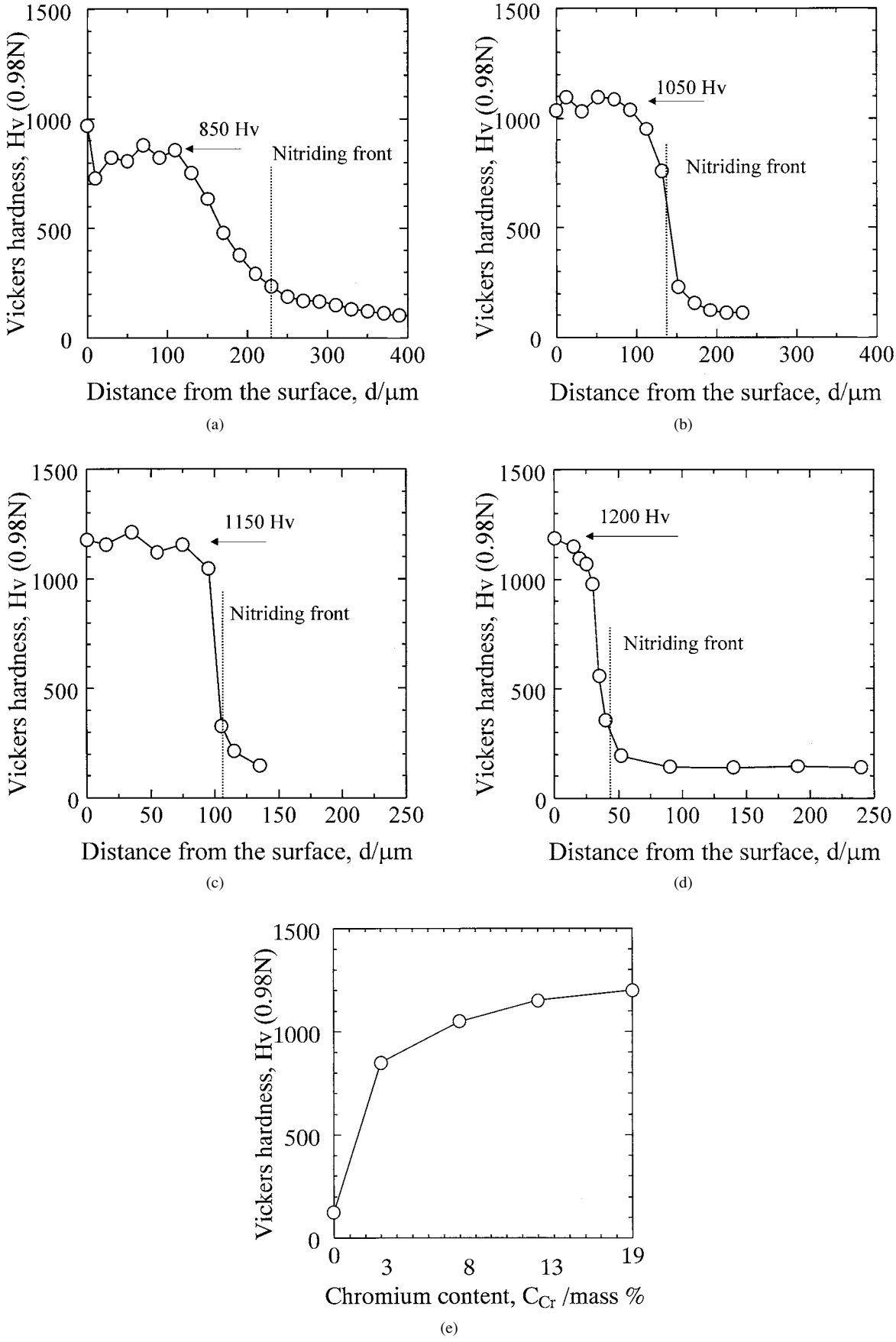

Figure 2 Hardness profile on the cross section of Fe-Cr alloys after plasma nitrided at 773 K for 57.6 ks. (a) Fe-3Cr alloy, (b) Fe-8Cr alloy, (c) Fe-13Cr alloy, (d) Fe-19Cr alloy (e) Variation of average hardness in the nitrided layer with increasing the chromium content.

TABLE III Mass of constituent and calculated volume fraction for four nitrided alloys

Specimen	Mass% CrN	Mass% Fe	f
Fe-3Cr	3.78	97.020	0.048
Fe-8Cr	10.1	92.030	0.124
Fe-13Cr	17.3	86.320	0.206
Fe-19Cr	23.6	81.360	0.272

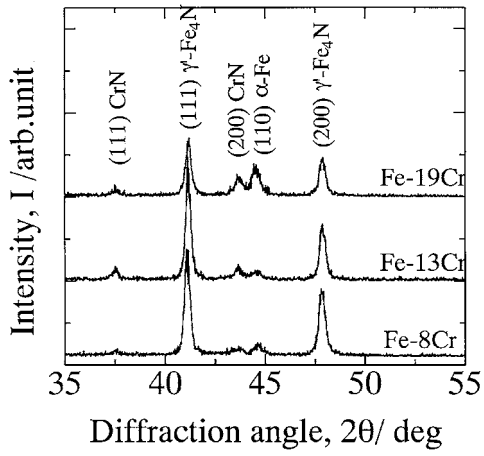

Figure 3 XRD pattern on the surface of Fe-Cr alloys after plasma nitrided at 823 K for 90 ks.

mainly consisted of γ'-Fe_4N as an iron nitride. Relative intensity of CrN to γ'-Fe_4N increases with chromium contents. This might be because of gradual increase of CrN volume fraction with chromium content. Assuming that all chromium formed CrN during nitriding, then volume fraction of CrN, f_{nitride} can be calculated as follows:

$$f_{\text{nitride}} = \frac{\rho_{\text{Fe}} \cdot m_{\text{nitride}}}{\rho_{\text{nitride}} \cdot m_{\text{Fe}} + \rho_{\text{Fe}} \cdot m_{\text{nitride}}} \qquad (1)$$

where ρ is the density of mass, and m is the mass for each suffix constituent in the alloy. Table III summarized the measured mass of constituent and the calculated CrN volume fraction for four nitrided alloys. Hence, volume fraction of CrN in Fe-19 Cr can be estimated by $f_{\text{nitride}} = 0.272$. In the similar manner, the volume fraction of Fe-13Cr, Fe-8Cr and Fe-3Cr are calculated for 0.206, 0.124 and 0.048, respectively. It is clear that f_{nitride} increased with chromium content.

3.2. Plasma nitriding of Fe-Cr alloys at high temperature

Plasma nitriding at $T = 873$ K has been carried out to investigate the effect of nitriding temperature on microstructure of nitrided layers. The microstructure of the plasma nitrided specimens at this temperature becomes far from those shown in Fig. 1. As seen in Fig. 4, all the plasma nitrided specimens at 873 K for 176.4 ks (49 h) have an anormal microstructure. In the case of Fe-13Cr alloy, the internal nitriding layer was formed to be in stripe-pattern, where bright and dark layers alternatively appeared up to the thickness of 280–300 μm. The thickness of each layer in this stripe-pattern was 10–15 μm. Notice here that the nitriding front of each sub-layer aligns in parallel with the specimen surface. This demonstrates that these sub-layers might never be formed by local deformation of internal nitriding layer, but by diffusion controlled process during nitriding.

Plasma nitrided Fe-8Cr and Fe-19Cr also exhibited unusual nitrided layer. Nitrided layer is divided into two and three different sub-layers for Fe-8Cr and Fe-19Cr, respectively. This is because each sub-layer has different corrosion resistance in etching. In other words chromium concentration is different in each sub-layer. In Fe-3Cr, different chromium concentration was also observed at the vicinity of nitriding front.

Hardness profiles on the cross-section of four plasma nitrided specimens at 873 K for 176.4 ks (49 h) are compared with each other from Fig. 5a to d. Assuming that nitriding process is still nitrogen diffusion controlled, the hardness plateau value might be nearly constant within the nitrided layer and the hardness distribution profile be stretched toward the direction of depth since the diffusion process is activated with increasing the nitriding temperature from 773 K to 873 K. However, the measured hardness profiles are never resembling to those in Fig. 2, irrespective of chromium content. The measured hardness became lower with increasing the nitriding temperature. Even in Fe-19Cr, the maximum surface hardness was limited by about 900 Hv while it was 1200 Hv in Fig. 2d. Just as seen in Fig. 2d, location of nitriding front measured in Fig. 4d is also corresponding to the end of transition zone in the above hardness distribution.

Let us describe the hardness distribution more precisely. Fig. 5b and d show the measured hardness profiles on the cross-section of plasma nitrided Fe-8Cr and Fe-19Cr specimens. In the case of Fe-19Cr, even in the nitrided layer, hardness profile has three steps before decreasing down to the same level as the matrix hardness: $0 < d < 90$, $90 < d < 150$ and $150 < d < 230$ μm. These three steps are corresponding to three different etched layers in Fig. 4d. There are two steps in the plasma nitrided Fe-8Cr: $0 < d < 200$ and $0 < d < 360$ μm. These are also corresponding to two sub-layers observed in Fig. 5b. Fig. 5c shows the hardness profile on the cross-section of Fe-13Cr specimen. In the normal profile as shown in Fig. 2c, hardness becomes maximum at the vicinity of the surface, keeps constant in plateau and then decreases to matrix hardness. However, surface hardness of this plasma nitrided Fe-13Cr alloy is limited to 600 Hv, then gradually increases up to 1000 Hv near the nitriding front. In the above gradual increase of hardness in average, significant deviation of hardness by 180 Hv to 300 Hv can be seen in Fig. 5c. Templating one local variation hardness with a pitch of 15–20 μm in the depth, the hardness profile in the internal nitriding layer can be divided into eleven sub-layers. Remember that the interval between successive sub-layers in the stripe-pattern in Fig. 4c should be 15–20 μm. This wavy pattern in hardness profile is corresponding to the stripe-pattern of microstructure.

Fig. 6 shows X-ray diffraction pattern on the specimen surface of Fe-Cr alloys plasma nitrided at 873 K for

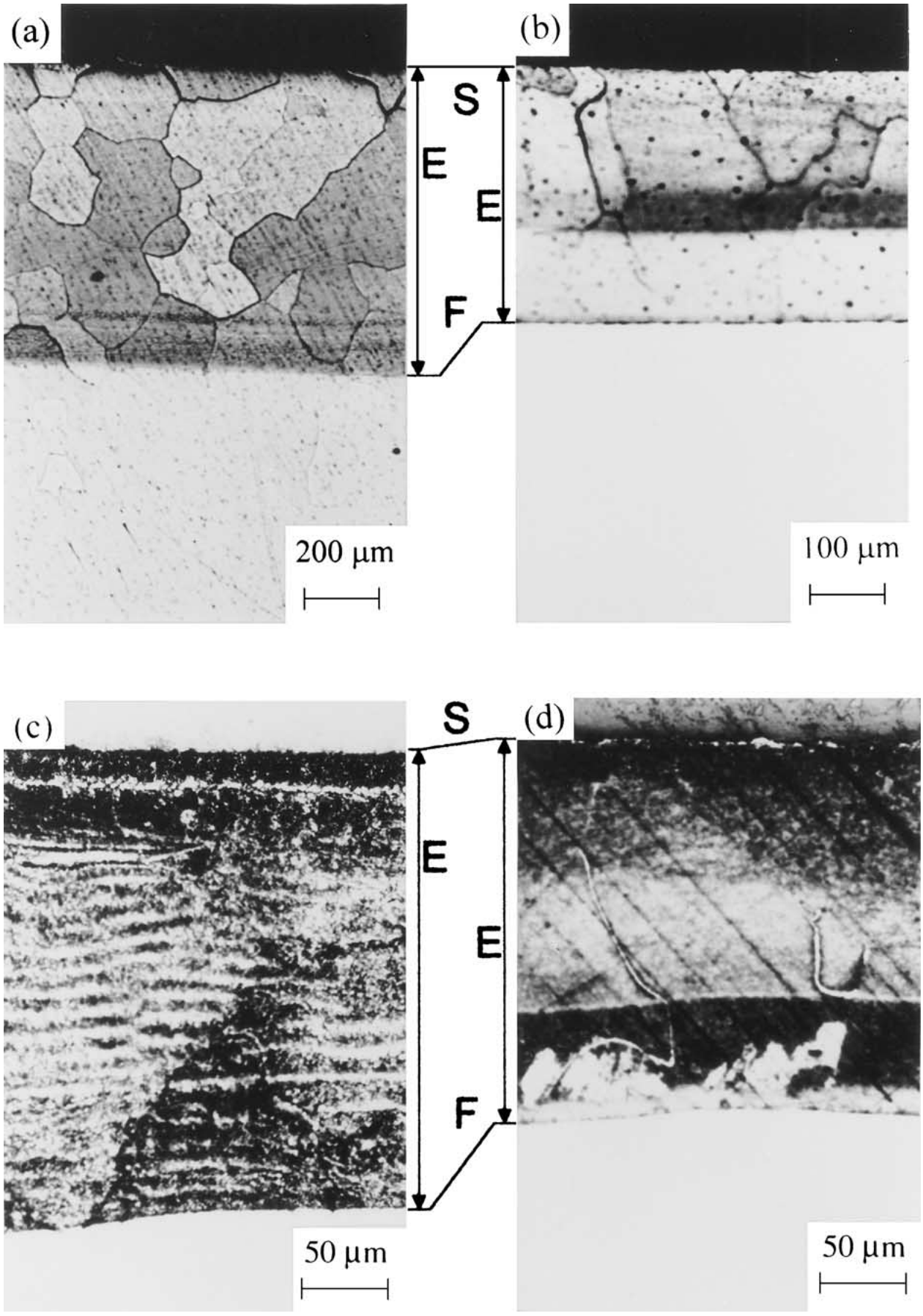

Figure 4 Microstructure of (a) Fe-3Cr, (b) Fe-8Cr, (c) Fe-13Cr and (d) Fe-19Cr alloys after plasma nitrided at 873 K for 176.4 ks.

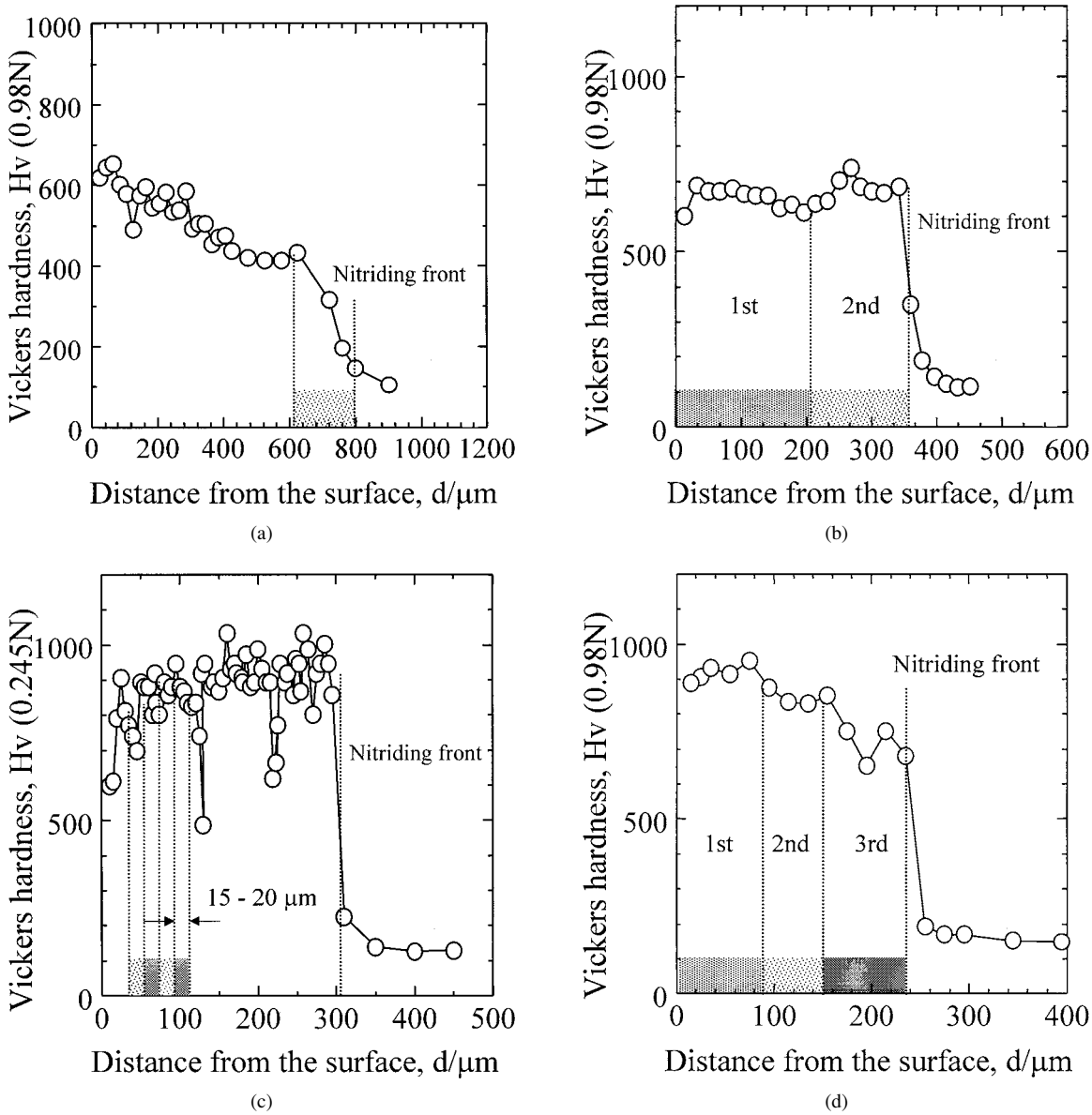

Figure 5 Hardness profile on the cross section of Fe-Cr alloys after plasma nitrided at 873 K for 176.4 ks. (a) Fe-3Cr alloy, (b) Fe-8Cr alloy, (c) Fe-13Cr alloy, (d) Fe-19Cr alloy.

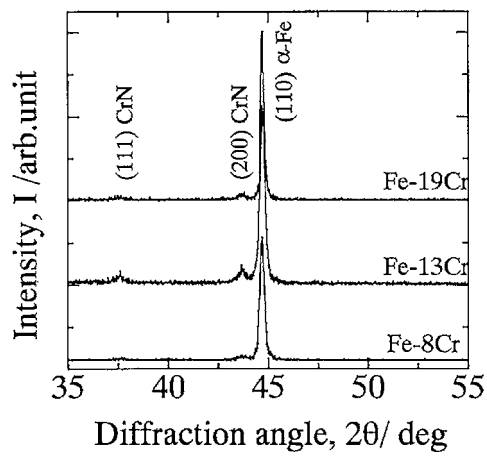

Figure 6 XRD pattern on the surface of Fe-Cr alloys after plasma nitrided at 873 K for 176.4 ks.

176.4 ks (49 h). Strong peaks of α-Fe, and small peaks of CrN were detected over specimen surface. Hence, in the case of plasma nitriding at $T = 873$ K, no external nitriding layer i.e γ'-Fe_4N formed during nitriding.

4. Discussions

Hardness profile of plasma nitrided Fe-Cr alloys at the temperature range of 773 to 823 K can be explained only by nitrogen diffusion process; the growth of nitrided layer is mainly controlled by diffusion of nitrogen in alloys [6, 11]. Nitrogen atoms diffuse into specimens during nitriding, and firstly react with chromium, which has higher affinity to nitrogen rather than iron. Hence, precipitation of chromium nitride is selected in Fe-Cr system, and with a further increase of nitrogen in solid solution, iron nitride can be also formed. Formation of the chromium nitrides usually increases the hardness of steels. As had been discussed in Ref. [12], the hardness of nitrided layer increases in proportion to the square root of nitride volume fraction, f. Volume fraction of CrN can be calculated under the assumption that all chromium atoms were reacted into CrN during nitriding. Fig. 7 depicts an increase of hardness ΔHv ($\equiv$[measured hardness] $-$ [matrix hardness]) with increasing the volume fraction of CrN. As reported in Ref. [13], $\Delta Hv \propto f^{1/2}$ for Fe-Ti alloys since the nitrided Fe-Ti alloys are strengthened by precipitation

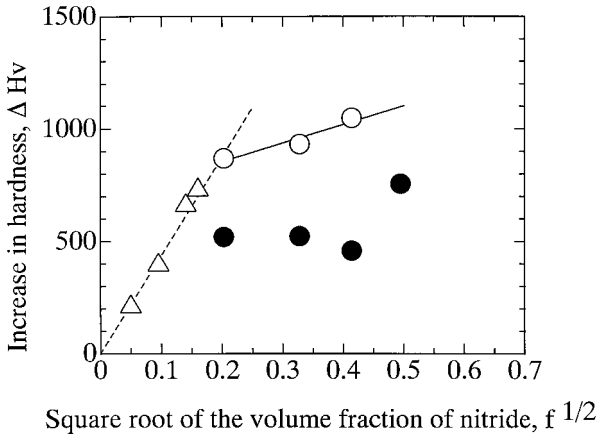

Figure 7 The relationship between volume fraction of chromium nitride and increase in hardness. O: Fe-Cr at 773 K, △: Fe-Ti [13], ●: Fe-Cr at 873 K.

of TiN. For low chromium content alloy like Fe-3Cr, strengthening mechanism is still governed by precipitation of CrN since linear $\Delta Hv \propto f^{1/2}$ relation is still held on for Fe-3Cr. Although ΔHv for Fe-3Cr is still proportional to $f^{1/2}$ for Fe-xCr ($x \geq 8$), the measured ΔHv values were not on the extrapolated line in $\Delta Hv - f^{1/2}$ for Fe-Ti alloys. The different slope from extrapolated line for Fe-xCr($x \geq 8$), reveals that other strengthening mechanism works for Fe-xCr ($x \geq 8$). As pointed out in Ref [12], when $R/b < 20$ for the diameter R of CrN and the Burgers vector b, the shearing mechanism of dislocation governs the strengthening process even for Fe-3Cr. Since $R/b > 20$ for the higher chromium content alloys, Orowan bypath mechanism becomes dominant since the bowing dislocation is constrained by the CrN precipitates [14].

The volume fraction of CrN formed also reflects on the hardness profile of nitrided layers. In Fe-3Cr, in comparison with other alloys (Fe-8Cr, Fe-13Cr, Fe-19Cr), small volume fraction of chromium gives relatively large diffusion effective cross-section area, and then results in that the dissolved nitrogen can penetrate into the matrix with few obstacles. Since dissolved nitrogen decreases exponentially toward the matrix, the dissolved chromium still remain in the matrix at the nitriding front. Hence, the hardness gradually decreased with nitrogen concentration. On the other hand, in high chromium content alloys, relative small diffusion effective cross-section area reduces penetrating mass of dissolved nitrogen mass in the matrix.

Compared with the normal microstructure and corresponding strengthening mechanism for plasma nitrided for 773 K to 873 K, anormal microstructure observed in the plasma nitrided specimens at 873 K cannot be described by the above nitriding mechanism. This anormality reflects on the relationship between ΔHv and $f^{1/2}$ in Fig. 7. Hence, these microstructures and strengthening mechanism behavior seems to be difficult to explain only by considering the nitrogen-diffusion-controlled mechanism in nitriding.

Concerning with the growth of nitrided layer in the present study, as similar to the previous studies [6, 13, 14], the relation between the thickness of internal nitrding layer, E, and nitriding time, t, can be expressed by parabolic law as the follow:

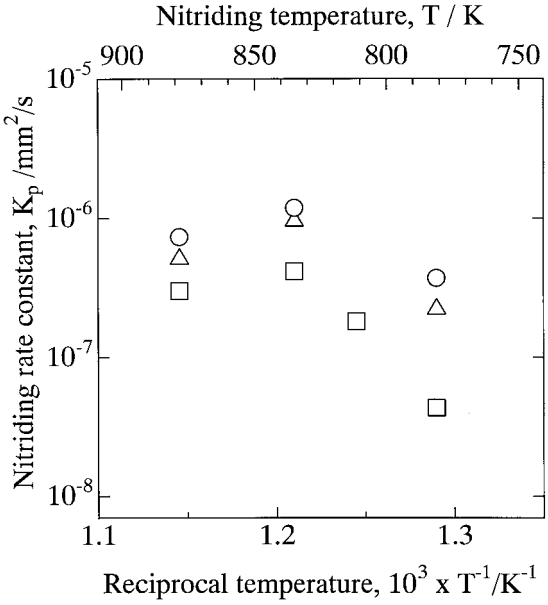

Figure 8 Temperature dependence of nitriding front rate constant of Fe-Cr alloys. O: Fe-8Cr, △: Fe-13Cr, □: Fe-19Cr.

$$E^2 = K_P \cdot t, \tag{2}$$

where K_P is the growth rate constant of nitriding front during plasma nitriding. Temperature dependence of K_P for each alloy is shown in Fig. 8. K_P increased with chromium content. Moreover, for the same chromium content, K_P increased with temperature until $T = 823$ K, but then decreased at $T = 873$ K. This behavior is described in later.

Growth rate of nitriding front for plasma nitrided Fe-Cr alloys can be usually explained using Wagner's rate equation of internal oxidation [15]. Since CrN precipitates with the concentration of $N_B$in the internal nitriding layer, the relation between thickness of nitrided layer, E, and nitriding time, t, can be written as follows:

$$E^2 = \frac{2N_N^S D^{app}}{\nu N_B} \cdot t \tag{3}$$

where D^{app} is the apparent diffusion coefficient of nitrogen in the internal nitriding layer, $N_N{}^S$ the nitrogen concentration at the specimen surface, N_B the concentration of alloying element in the internal nitriding layer, and ν the molar ratio of alloying element to nitrogen in nitride precipitation, respectively. All chromium atoms are assumed to be in CrN, and then $\nu = 1$ and N_B becomes the chromium content in the present work. Equations 2 and 3 provide:

$$K_P = \frac{2N_N^S D^{app}}{N_B}. \tag{4}$$

This reveals that K_P decreases with increasing N_B.

In general, temperature dependence of diffusion coefficient can be expressed by Arrhenius reaction rate. Hence, the temperature dependence of apparent diffusion coefficient of nitrogen, D^{app}, can be written as follows:

$$D^{app} = A \exp\left[-\frac{Q^{app}}{RT}\right]. \quad (5)$$

In the similar way, diffusion coefficient of nitrogen in pure Fe, $D_N{}^{Fe}$ can be also expressed as follows:

$$D_N^{Fe} = B \exp\left[-\frac{Q_N^{Fe}}{RT}\right] \quad (6)$$

and, after Grieveson and Turkdogan [16]

$$D_N^{Fe} = 6.20 \times 10^{-7} \exp\left\{-\frac{[77.7 \pm 7.8](\text{kJ/mol})}{RT}\right\} (\text{m}^2/\text{s}).$$

Using Equations 5 and 6, ratio of D^{app} to $D_N{}^{Fe}$ is obtained as follows:

$$\frac{D_N^{app}}{D_N^{Fe}} = C \exp\left[-\frac{(Q^{app} - Q_N^{Fe})}{RT}\right]. \quad (7)$$

Replacing $(Q^{app} - Q_N{}^{Fe})$ with Q^*, Equation 8 should be rewriting:

$$\frac{D_N^{app}}{D_N^{Fe}} = C \exp\left[-\frac{Q^*}{RT}\right] \quad (8)$$

where Q^* indicates activation energy for formation of nitride precipitation in the nitriding layer. Considering that apparent diffusion coefficient of nitrogen should be lower due to Cr content in alloy, Q^* in Equation 8 should be related to Cr content. In the case of nitriding pure Fe, $Q^* = 0$: $D_N{}^{app}/D_N{}^{Fe} = 1$ means that apparent diffusion coefficient of nitrogen should be equal to that of nitrogen in pure Fe. This activation energy denotes excess energy barrier needed to drive more nitrogen solution against precipitation of Cr as CrN.

$D_N{}^{app}$ can be calculated from and experimental values of K_P, using the following equation:

$$D^{app} = \left[\frac{N_{Cr}}{2N_N}\right] K_P. \quad (9)$$

Table IV shows calculated $D_N{}^{app}$ for various Fe-Cr alloys at several temperatures in comparison with nitrogen diffusion in pure-Fe. As mentioned above, $D_N{}^{aap}$ decreased with Cr content at all temperatures, indicating that diffusion of nitrogen was disturbed by amount of Cr in alloy. Fig. 9 shows the relation between nitriding temperature and ratio of $D_N{}^{app}/D_N{}^{Fe}$ for various chromium contents. $D_N{}^{app}/D_N{}^{Fe}$ increased with

TABLE IV Apparent diffusion coefficient of N in Fe-Cr alloys as calculated at several temperatures in comparison with pure-Fe

	$D_N{}^{app}$ (m^2/s)		
Specimen	773 K	823 K	873 K
Pure-Fe	3.3×10^{-12}	6.87×10^{-12}	1.31×10^{-11}
Fe-8Cr	1.92×10^{-12}	6.161×10^{-12}	3.82×10^{-12}
Fe-13Cr	7.61×10^{-13}	3.27×10^{-12}	1.75×10^{-12}
Fe-19Cr	9.57×10^{-14}	9.13×10^{-13}	6.62×10^{-13}

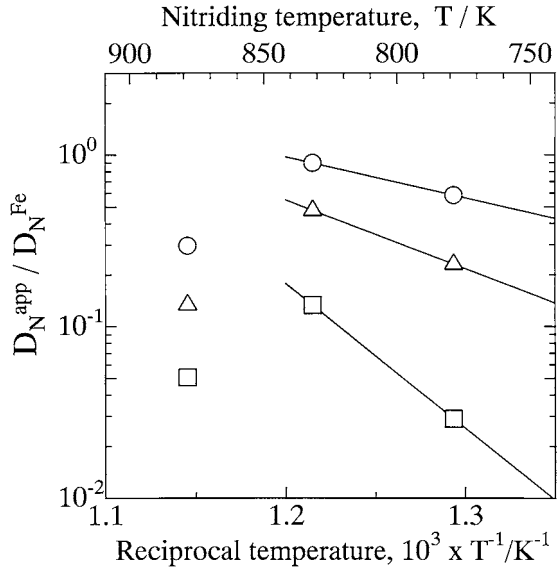

Figure 9 Relation between nitriding temperature and ratio of apparent nitrogen diffusion coefficient to nitrogen diffusion coefficient in pure-Fe ($D_N{}^{app}/D_N{}^{Fe}$) O: Fe-8Cr, Δ: Fe-13Cr, □: Fe-19Cr.

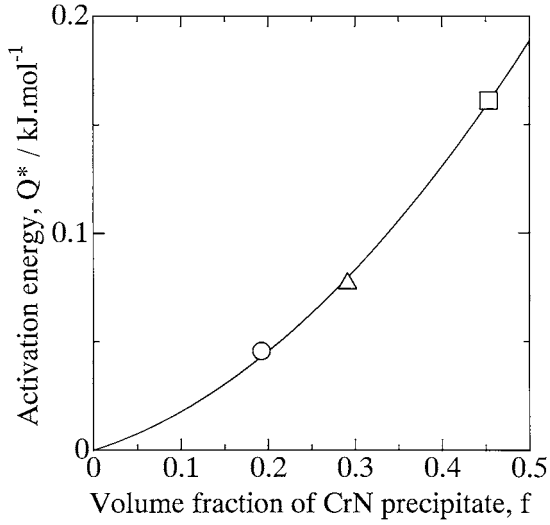

Figure 10 Relation between activation energy Q^* and change in volume fraction of CrN. O: Fe-8Cr, Δ: Fe-13Cr, □: Fe-19Cr.

decreasing the chromium concentration and increasing temperature, up to 823 K. Using Equation 8, for temperature up to 823 K, activation energy Q^* was obtained for each alloy. Fig 10 shows the variation of Q^* with the volume fraction of CrN. Activation energy increases with increasing the volume fraction of CrN. Nitrogen effective diffusion area decreases as CrN formed during nitriding. Hence, apparent diffusion coefficient of nitrogen, $D_N{}^{app}$, became smaller as higher chromium content.

$D_N{}^{app}/D_N{}^{Fe}$ at nitriding temperature of $T = 873$ K became relatively small for all alloys than the extrapolated values from the lower temperature side. Hence, nitriding behavior at 873 K can not be explained only using nitrogen diffusion mechanism as described above. Another factor must be considered for slowing apparent diffusion of nitrogen at this nitriding temperature. As listed in Table V, diffusion coefficient of chromium increases nearly 7.5 times from 823 K to

TABLE V Diffusion coefficient of N and Cr in α-Fe as calculated at several temperatures [17]

Diffusion coefficient	Temperature		
	773 K	823 K	873 K
D_N (cm^2/s)	3.3×10^{-8}	6.87×10^{-8}	1.305×10^{-7}
D_{Cr} (cm^2/s)	0.136×10^{-15}	1.323×10^{-15}	9.92×10^{-15}

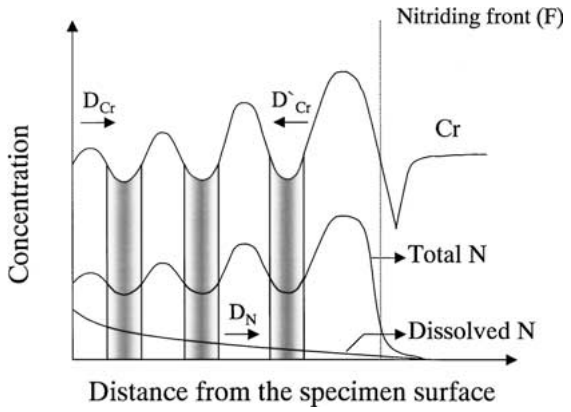

Figure 11 Schematic illustration of mutual diffusion of nitrogen and chromium during nitriding.

873 K but still too low, while diffusion coefficient of nitrogen increases only 1.8 times in the same temperatures range. Hence, chromium is never expected to diffuse in the whole range of nitrided area, but local diffusion of chromium must be also taken into account. The mechanism of nitrogen diffusion collaborated with local chromium diffusion on formation of stripe-pattern microstructure can be explained qualitatively as be described in Fig. 11. This figure schematically depicts a spatial relationship between nitrogen-chromium diffusion and reactive formation of CrN. Once the reaction by $Cr + N \rightarrow CrN$ takes at the specified point F (nitriding front), the chromium concentration decreases at the vicinity of F. This deficiency of chromium activates the diffusion chromium process in local at 873 K. Since the reactivity to CrN is also enhanced at much presence of chromium at the vicinity of F, the above process is thought to work in the cascading manner: (reaction to CrN) $\rightarrow$ (deficiency of Cr) $\rightarrow$ (local diffusion of Cr) $\rightarrow$ (continued reaction to CrN) $\rightarrow$ .... Hence, the above chained-routine must reflect on the local fluctuation of chromium content and local distribution of CrN.

The above mechanism works for the higher chromium content iron like Fe-19Cr, since larger amount of chromium becomes an obstacle that chromium is capturing diffusing nitrogen atom. The higher chromium iron alloy has many obstacles; the lower has a few obstacles.

To understand quantitatively the above anormal nitriding behavior, more detailed study of interaction among dissolved chromium, diffusing chromium and nitrogen, precipitating nitride of CrN should be required from the standing point of thermodynamics and kinetics of growing nitriding layer in concerned with stress or strain fields due to precipitate nitride.

5. Conclusions

Plasma nitriding of Fe-Cr alloys in temperature range of 773–873 K has been performed in order to provide a new type of nitrided layer microstructures through diffusion control of both nitrogen and chromium.

Plasma nitriding of Fe-Cr alloys in low temperature region results in typical hardness profile on the cross section of specimens. In the low chromium content alloys, the graded hardness profile can be realized by gradual decrease of volume fraction of CrN precipitation. In this temperature region, formation of nitrided layer microstructure can be explained only by diffusion of nitrogen during nitriding.

Plasma nitriding of high chromium content alloys at relatively high temperature region ($T = 873$ K), results in the stripe-pattern microstructure of nitrided layers. This microstructural pattern formation strictly depends on chromium content in alloy. These anormal nitrided microstructures significantly reflect on the mechanical properties.

Further study is on progress to investigate the relation between fine-layered system in microstructure and wear toughness/impact wear resistance. A new type nitrided microstructure or a sandwiched structure of soft and hard layers is expected to play a role of deformable mechanical dumper or spring, to elastically absorb the externally applied displacement by heavy impact load.

References

1. B. EDENHOFER, "Heat Treatment of Metals" (1974) p. 23.
2. G. J. DIXON, S. A. PLUMB and H. C. CHILD, *Heat Treatment* **81** (1983) 137.
3. A. DA SILVA ROCHA, T. STROHAECKER, V. TOMALA and T. HIRSCH, *Surface and Coating Technology* **115** (1999) 24.
4. J. M. PRIEST, M. J. BALDWIN, M. P. FEWELL, S. C. HAYDON, G. A. COLLINS, K. T. SHORT and J. TENDYS, *Thin Solids Films* **345** (1999) 113.
5. C. ALVES JR., J. A. RODRIGUES and A. E. MARTINELLI, *Material Science and Engineering* **A2798** (2000) 10.
6. H. KUWAHARA, H. MATSUOKA, J. TAKADA, S. KIKUCHI, Y. TOMII and I. TAMURA, *Oxidation of Metals* **36** (1991) 146.
7. M. SAHARA, T. SATO, S. ITO and K. AKASHI, *Materials Chemistry and Physics* **54** (1998) 123.
8. M. UMA DEVI and O. N. MOHANTY, *Surface and Coatings Technology* **107** (1998) 55.
9. W. KOVACS and W. RUSSEL, in Proc. Int. Conf. Ion Nitriding, Cleveland, OH, 15–17 September 1986, (ASM International) p. 9.
10. B. PODGORNIK, J. VIZ INTIN and V. LESKOVSEK, *Surface and Coatings Technology* **108–109** (1998) 454.
11. L. E. KINDLIMANN and G. S. ANSELL, *Metal Trans.* **1** (1970) 163.
12. V. GEROLD and H. HARBELKORN, *Phys. Stat. Sol.* **16** (1966) 675.
13. H. KUWAHARA and J. TAKADA, *J. Jpn. Powder and Powder Metallurgy* **41** (1994) 1345.
14. H. KUWAHARA, PhD thesis, Kyoto University, 1992 p. 60.
15. C. WAGNER, *Z. Electrochem.* **63** (1959) 772.
16. P. GRIEVESON and E. T. TURKDOGAN, *Trans. AIME* **230** (1964) 1604.
17. Japan Institute of Metals (ed.), "Metals Data Book" (Maruzen, Tokyo, 1974).

Received 19 June 2000
and accepted 2 October 2001